Lattice Effects on the Magnetoresistance in Doped $LaMnO_3$

H. Y. Hwang,[1,2] S-W. Cheong,[1] P. G. Radaelli,[3] M. Marezio,[1,4] and B. Batlogg[1]

[1]*AT&T Bell Laboratories, Murray Hill, New Jersey 07974*

[2]*Joseph Henry Laboratories of Physics, Princeton University, Princeton, New Jersey 08544*

[3]*Institute Laue-Langevin, BP 156, 38042 Grenoble Cedex 9, France*

[4]*Laboratoire de Cristallographie, Centre National de la Recherche Scientifique-UJF, BP 166, 38042 Grenoble Cedex 9, France*

(Received 22 March 1995)

A detailed study of doped $LaMnO_3$ with fixed carrier concentration reveals a direct relationship between the Curie temperature T_c and the average ionic radius of the La site $\langle r_A \rangle$, which is varied by substituting different rare earth ions for La. With decreasing $\langle r_A \rangle$, magnetic order and significant magnetoresistance occur at lower temperatures with increasing thermal hysteresis, and the magnitude of the magnetoresistance increases dramatically. These results show that the notion of "double exchange" must be generalized to include changes in the Mn-Mn electronic hopping parameter as a result of changes in the Mn-O-Mn bond angle.

PACS numbers: 72.15.Gd, 75.30.Kz, 75.50.Cc

There is renewed interest in manganese perovskites due to the magnetoresistance exhibited near the ferromagnetic ordering of Mn spins, which is accompanied by a large increase in electrical conductivity σ [1–3]. An issue of considerable importance, both for potential applications and for microscopic understanding, is resolving what principal factors determine the Curie temperature T_c and the magnetoresistance. Several different studies have shown that T_c and magnetoresistance are optimized when ~30% of the Mn^{+3} is converted to Mn^{+4} (e.g., by substituting divalent ions for La^{+3}) [1,4]. Yet even for this "hole doping" range there are large variations in the observed T_c and in the magnitude of the reported magnetoresistance. These discrepancies have been ascribed to chemical disorder, oxygen deficiencies, grain boundary effects, lattice constant effects, etc.

The magnetic and electronic properties have traditionally been examined within the framework of "double exchange," which considers the magnetic coupling between Mn^{+3} and Mn^{+4} that results from the motion of an electron between the two partially filled d shells with strong on-site Hund's coupling [5,6]. Using a simplified double exchange Hamiltonian, a recent calculation of the magnetic field dependent resistivity near the transition is found to be inconsistent with experimental results, and the authors propose that strong Jahn-Teller type electron-phonon coupling plays an important role [7]. Experimentally, it has been found that at a particularly tuned composition ($La_{0.83}Sr_{0.17}MnO_3$), where T_c and a trigonal to orthorhombic transition temperature coincide, the structural phase transition can be driven by an external magnetic field [8]. These results suggest that there is considerable coupling between magnetism and the lattice in this system.

In the perovskite $LaMnO_3$, the Mn ions occupy the B site and are surrounded by oxygen octahedra, which share corners to form a three-dimensional network, while the La ions occupy the A site between these octahedra. In several perovskites, the overlap between B-site d orbitals and oxygen p orbitals forms the electronically active band, and this overlap can be strongly influenced by the internal pressure generated by A-site substitution with ions of different radii [9]. With this notion in mind we have examined a series of samples in which the average ionic radius of the A site $\langle r_A \rangle$ is systematically varied while keeping the Mn^{+3}/Mn^{+4} ratio fixed at 7/3. We find that for decreasing $\langle r_A \rangle$, T_c decreases and the size of the magnetoresistance near T_c increases drastically. The magnetic transition remains sharp and becomes increasingly hysteretic in temperature with decreasing $\langle r_A \rangle$, indicating that this is a first order phase transition. We find that the principal effect of decreasing $\langle r_A \rangle$ is to decrease the Mn-O-Mn bond angle, thereby reducing the matrix element b which described electron hopping between Mn sites. This response to a reduction of $\langle r_A \rangle$, characteristic of perovskites, gives the counterintuitive result that b decreases as the Mn ions get closer to each other. This is corroborated by the systematic decrease of the high temperature conductivity and of T_c. We have explored the temperature phase diagram as a function of $\langle r_A \rangle$ and have identified an apparent maximum T_c of ~365 K for hole carrier doping fixed at 30%.

Polycrystalline samples of the $A_{0.7}A'_{0.3}MnO_3$ system (A is a trivalent rare earth ion and A' is a divalent alkali earth ion) were prepared through conventional solid-state reaction processing in air. Powder x-ray diffraction showed clean single-phase patterns. The oxygen content was found to be stable for various heat treatments (annealing in 200 bars oxygen at 650 °C, quenching from 1400 °C in air). Other studies on polycrystalline materials prepared in the same way have examined the oxygen content and found $Pr_{0.7}Ca_{0.3}MnO_{2.98\pm0.01}$ by chemical analysis, and $La_{0.67}Ba_{0.33}MnO_{2.99}$ by iodometric titration [10,11]. Resistivity ρ was measured using the standard four probe technique, and magnetization was

 0031-9007/95/75(5)/914(4)$06.00

measured using a commercial magnetometer (Quantum Design). The crystal structures of four of our samples were refined from powder neutron data analyzed by the Rietveld method. The data were collected with the D2B diffractometer of the Laue-Langevin Institute in the high intensity mode using a wavelength of 1.594 Å.

In the top panel of Fig. 1, $\log\rho(T)$ is shown at 0 and 5 T for 8 samples of $La_{0.7-x}Pr_xCa_{0.3}MnO_3$ for $x = 0, 0.175, 0.35, 0.525, 0.6, 0.7$ and $La_{0.7-y}Y_yCa_{0.3}MnO_3$ for $y = 0.35$ and 0.5. Since the ionic radius of La is greater than that of Pr which is in turn greater than that of Y, $\langle r_A\rangle$ monotonically decreases in this series of samples while the carrier concentration remains fixed. Decreasing $\langle r_A\rangle$ causes a decrease in T_c and an increase in the magnitude of the drop in ρ at T_c. Note that for $x = 0.7$, ρ appears to be insulating to lowest temperatures, while in 5 T there is a field-induced transition to metallic behavior, giving rise to enormous magnetoresistance [12,13]. For $y = 0.35$ and 0.5, ρ is always insulating in both 0 and 5 T, although for $y = 0.35$ there is a feature at ~60 K in 5 T which seems consistent with the systematic trend in ρ_{5T} with decreasing $\langle r_A\rangle$. In the bottom panel of Fig. 1, the magnetoresistance is specified as $\log(\rho_{0T} - \rho_{5T})/\rho_{5T}$ for data taken while cooling. The temperature for the maximum magnetoresistance correlates well with the peak in ρ_{0T} (shown with arrows). With the reduction of $\langle r_A\rangle$, T_c decreases monotonically and the magnitude of the magnetoresistance is enhanced dramatically.

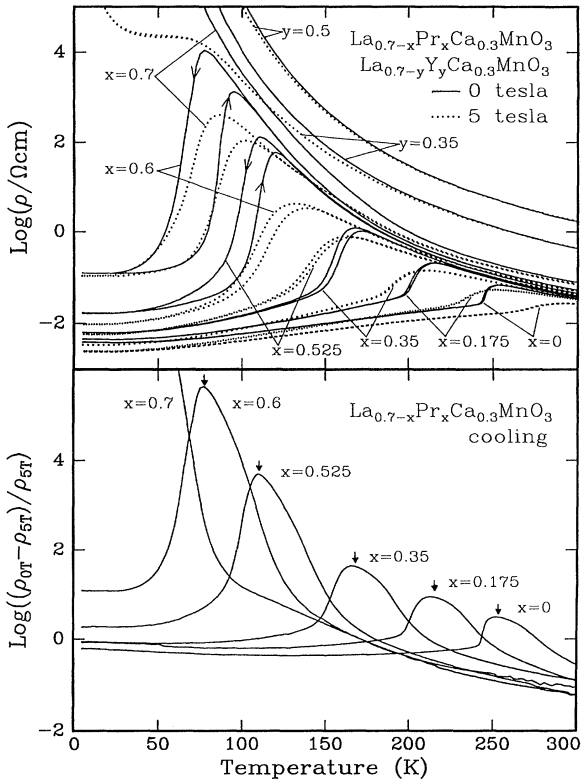

FIG. 1. Top panel: $\log\rho(T)$ in 0 and 5 T for a series of samples $La_{0.7-x}Pr_xCa_{0.3}MnO_3$ for $x = 0, 0.175, 0.35, 0.525, 0.6, 0.7$ and $La_{0.7-y}Y_yCa_{0.3}MnO_3$ for $y = 0.35$ and 0.5. Bottom panel: Magnetoresistance (cooling data) for $x = 0, 0.175, 0.35, 0.525, 0.6, 0.7$ specified as $\log(\rho_{0T} - \rho_{5T})/\rho_{5T}$, with the maximum in ρ_{0T} indicated by arrows.

There are several observations that emerge from the examination of $\rho(T)$ for varying $\langle r_A\rangle$. With decreasing $\langle r_A\rangle$, $\rho(T)$ is increasingly hysteretic in temperature in both 0 and 5 T. Indeed, the transition in 5 T resembles the transition in 0 T, simply shifted up in temperature and somewhat broader. Another aspect of Fig. 1 is that $\rho(T)$ above the transition is virtually identical for all the samples, the only difference being that the magnitude slowly increases with decreasing $\langle r_A\rangle$. This suggests that the nature of charge transport in the nonmetallic state above T_c is the same, and the difference simply reflects a reduction in b. In order to explore this idea, $\rho(300\text{ K})$ as a function of $\langle r_A\rangle$ is given in Fig. 2. ($\langle r_A\rangle$ is calculated from tabulated values [14].) $\rho(300\text{ K})$ increases with decreasing $\langle r_A\rangle$, with a sharp upturn near the composition for which ρ_{0T} remains insulating to lowest temperatures. The inset to Fig. 2 displays the close relationship between $\sigma(300\text{ K})$ and T_c^ρ [defined as the maximum in $d\log(\rho)/dT$], with $\langle r_A\rangle$ as the implicit parameter. This is just what one would expect from the basic concept of double exchange: both T_c and $\sigma(300\text{ K})$ reflect real charge motion determined by the Mn-Mn electron hopping rate.

The temperature dependent magnetization for these samples is given in the top panel of Fig. 3 at 100 Oe for both zero field cooled (ZFC) and field cooled (FC) runs. All measurements displayed are warming curves, although thermal hysteresis was also seen in the magnetization. The onset of ferromagnetism [T_c^M, defined as a minimum in $d(M/H)/dT$] correlates well with T_c^ρ seen in 0 field for $x = 0$, 0.175, 0.35, 0.525, and 0.6. In the

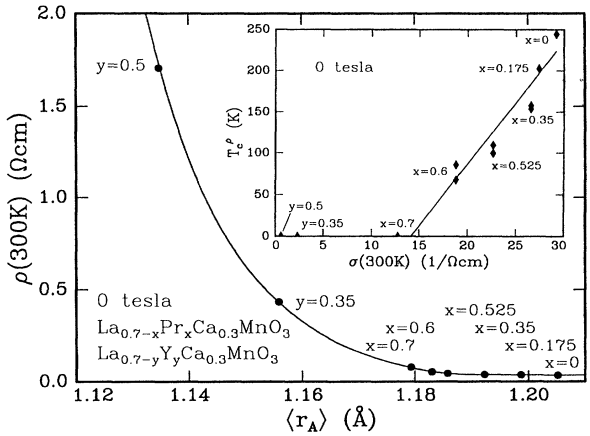

FIG. 2. $\rho(300\text{ K})$ in 0 T vs average ionic radius of the A site $\langle r_A\rangle$. Inset: T_c^ρ [defined as the maximum in $d\log(\rho)/dT$] vs $\sigma(300\text{ K})$ in 0 T.

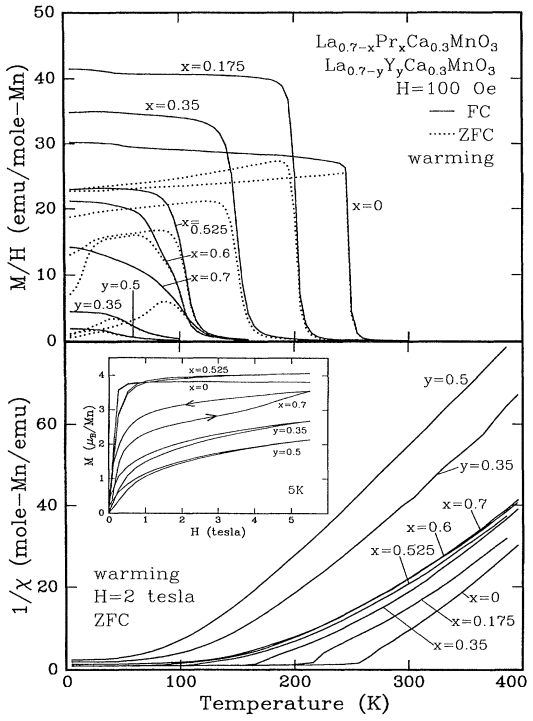

FIG. 3. Top panel: Temperature dependent magnetization (warming curves), taken both zero field cooled (ZFC) and field cooled (FC) at 100 Oe. Bottom panel: Temperature dependence of $1/\chi$ taken ZFC (warming curves) at 2 T. Inset: Magnetization curves taken at 5 K.

bottom panel of Fig. 3, $1/\chi$ as a function of temperature is shown for measurements taken ZFC in 2 T. The main result is a shift of $1/\chi$ to lower temperatures as $\langle r_A \rangle$ decreases, indicating a decrease of the overall magnetic interaction J_{DE} between the Mn moments.

Insight into the spin structure can be gained from measurements of the magnetization as a function of the applied field at 5 K (inset to Fig. 3). For $x = 0$, the response is that of a ferromagnet with a saturated moment close to that expected for the full Mn moment of $\sim 4.3 \mu_B$. However, as $\langle r_A \rangle$ decreases, there is a gradual trend toward reduced magnetization, and there is no evidence of saturation up to 5.5 T. These phenomena can be interpreted as a gradual canting of the moments with decreasing $\langle r_A \rangle$. The competition between double exchange ferromagnetism (FM) and exchange antiferromagnetism (AF) in layered antiferromagnets can result in canted antiferromagnetism as well as simple FM and AF [6]. Particularly the magnetization for $x = 0.7$ is suggestive of an irreversible increase in canting for fields higher than ~ 3 T.

The results discussed above indicate that the most important parameter in determining T_c for a given carrier concentration is $\langle r_A \rangle$. A more general discussion of this dependence on $\langle r_A \rangle$ invokes the "tolerance factor," a geometrical quantity defined as $t = (d_{A-O})/\sqrt{2}(d_{Mn-O})$. This factor t is a simple characterization of the size mismatch that occurs when the A-site ions are too small to fill the space in the three-dimensional network of MnO_6 octahedra. For a perfect size match ($t = 1$), the Mn-O-Mn bond angle (θ) would be 180°. For $t < 1$, rather than a simple contraction of bond distances, the octahedra tilt and rotate to reduce the excess space around the A site, resulting in $\theta < 180°$. The apparent decrease in b with decreasing $\langle r_A \rangle$ (and therefore decreasing t) originates from the decrease in θ. This relationship between θ and $\langle r_A \rangle$ has been confirmed for our samples by powder neutron diffraction at room temperature (see Table I).

To further elucidate the role of t and to establish a generalized phase diagram, we have explored a larger region of $\langle r_A \rangle$ values by studying additional compounds, varying the A and A' ions while keeping the carrier concentration fixed at 30% hole doping. Our results are given in the phase diagram shown in Fig. 4. (t is calculated from tabulated values [14].) Three principal regions are delineated: a paramagnetic insulator, a ferromagnetic metal, and a ferromagnetic insulator. In this phase diagram there is an apparent maximum in T_c which occurs around $t = 0.93$, an issue that is of interest for considering technological applications. The slight decrease in T_c beyond $t = 0.93$ may be related with the crossover from orthorhombic to trigonal structure, or it may be due to the increased size mismatch between the A and A' ions.

The influence of t on magnetic properties is well established for superexchange antiferromagnets such as $AFeO_3$, where A is a trivalent rare earth ion [15]. Analysis of this system has shown that the Néel temperature is directly proportional to $\cos^2\phi$ (ϕ is the Fe-O-Fe bond angle),

TABLE I. Selected structural parameters at room temperature. In the orthorhombic structure, there are two distinct oxygen sites: the out-of-plane O_1 and the planar O_2.

A site	$Pr_{0.7}Ca_{0.3}$	$La_{0.525}Pr_{0.175}Ca_{0.3}$	$La_{0.7}Sr_{0.3}$	$La_{0.7}Ba_{0.18}Sr_{0.12}$
Structure	Orthorhombic	Orthorhombic	Trigonal	Trigonal
d_{Mn-Mn}(Å)	3.855	3.868	3.887	3.904
d_{Mn-O_1}(Å)	1.964	1.966	1.957	1.962
d_{Mn-O_2}(Å)	1.976, 1.967	1.979, 1.951	...	...
θ_{Mn-O_1-Mn}	156.5	158.4	166.3	168.5
θ_{Mn-O_2-Mn}	156.4	160.0	...	...
$\langle r_A \rangle$	1.179	1.199	1.244	1.273

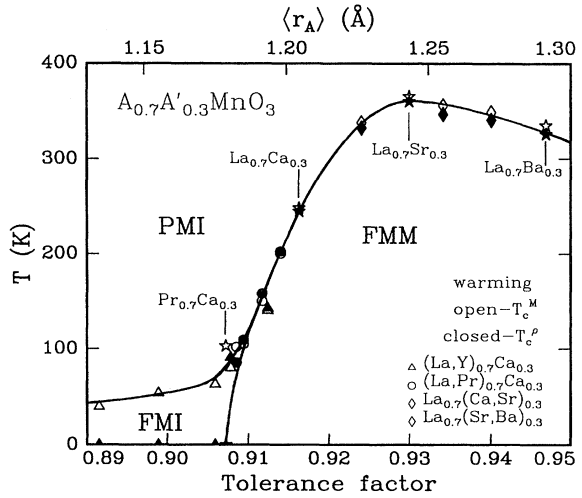

FIG. 4. Phase diagram of temperature vs tolerance factor for the system $A_{0.7}A'_{0.3}MnO_3$, where A is a trivalent rare earth ion and A' is a divalent alkali earth ion. Open symbols denote T_c^M measured at 100 Oe. Closed symbols denote T_c^ρ. Data taken while warming.

consistent with the b^2 dependence of the superexchange interaction. More recently, the connection between t and charge transport has been found in $ANiO_3$ [16]. By increasing t or temperature a first order insulator-metal transition occurs. This transition is accompanied by a slight ($\sim$0.2%) reduction in unit cell volume, which appears to cause a sudden increase in the one-electron bandwidth. This points to an important aspect of the manganese perovskites that has not yet been considered: the change of b as a result of magnetic order. From the temperature hysteresis in ρ evident in Fig. 1, the transition at T_c appears to be first order, and involves a switching from a generic nonmetallic state to a metallic state, reminiscent of the transition in $ANiO_3$. Critical point calculations around a ferromagnetic transition for fixed J predict a much slower, smooth second order transition, completely incompatible with our results [17]. However, an abrupt increase in b at the first order transition would result in an abrupt increase in J_{DE}, consistent with what is observed.

The current study, together with previous results, shows that any realistic theoretical treatment must allow for variations in b as a result of changes in t, thermal expansion, structural changes, etc. In a general sense the transition at T_c involves not only magnetic ordering, but also a metal-insulator transition. A key problem with simplified double exchange calculations is the failure to describe the large change in electron scattering observed near T_c by just spin scattering at a second order ferromagnetic transition. The metal-insulator transition in $ANiO_3$ for a similar range of t suggests that the phase diagram of Fig. 4 is determined by an intrinsic electronic metal-insulator transition due to changes in b, independent of the double exchange interaction.

In summary, the present study of a range of manganese perovskites with fixed hole concentration has connected a reduction of T_c and an increase in magnetoresistance with a decrease in the microstructural Mn-O-Mn bond angle. While the notion of double exchange describes an important aspect of the magnetoresistance near T_c, these results demonstrate the need to consider changes in the electronic hopping element b as a result of changes in the lattice. This study in bulk materials, in conjunction with studies as a function of carrier concentration, is an appropriate starting ground for understanding the wide range of magnetic effects observed in thin films.

We would like to thank A. J. Millis, P. B. Littlewood, B. I. Shraiman, and N. P. Ong for helpful discussions.

[1] G. H. Jonker and J. H. Van Santen, Physica (Utrecht) **16**, 337 (1950); C. W. Searle and S. T. Wang, Can. J. Phys. **47**, 2703 (1969).
[2] R. von Helmholt *et al.*, Phys. Rev. Lett. **71**, 2331 (1993).
[3] S. Jin *et al.*, Science **264**, 413 (1994).
[4] P. Schiffer *et al.* (to be published).
[5] C. Zener, Phys. Rev. **82**, 403 (1951); P. W. Anderson and H. Hasegawa, Phys. Rev. **100**, 675 (1955).
[6] P.-G. de Gennes, Phys. Rev. **118**, 141 (1960).
[7] A. J. Millis, P. B. Littlewood, and B. I. Shraiman (to be published).
[8] A. Asamitsu *et al.*, Nature (London) **373**, 407 (1995).
[9] J. B. Goodenough and J. M. Longo, *Landolt-Börnstein Tabellen* (Springer, Berlin, 1970), Vol. III/4a.
[10] Z. Jirák *et al.*, J. Magn. Magn. Mater. **53**, 153 (1985).
[11] H. L. Ju *et al.*, Phys. Rev. B **51**, 6143 (1995).
[12] Y. Tomioka *et al.* (to be published).
[13] ρ grew too large to be measured below 50 K, but it appears to stay above 10^7 Ω cm to lowest temperatures.
[14] R. D. Shannon, Acta Crystallogr. Sect. A **32**, 751 (1976).
[15] D. Treves, M. Eibschütz, and P. Coppens, Phys. Lett. **18**, 216 (1965); G. A. Sawatzky, W. Geertsma, and C. Haas, J. Magn. Magn. Mater. **3**, 37 (1976).
[16] J. B. Torrance *et al.*, Phys. Rev. B **45**, 8209 (1992).
[17] M. E. Fisher and J. S. Langer, Phys. Rev. Lett. **20**, 665 (1968).